


## Article

# Optimization Study of Inert Gas Distribution for Multiple-Bay Fuel Tank

Lei Shao <sup>1,2,\*</sup> , Jiawei He <sup>1,2</sup>, Xia Lu <sup>3</sup> and Weihua Liu <sup>4</sup><sup>1</sup> School of Aeronautics, Chongqing Jiaotong University, Chongqing 400074, China<sup>2</sup> The Green Aerotechnics Research Institute of Chongqing Jiaotong University, Chongqing 401135, China<sup>3</sup> AVIC Hefei Jianghuai Aircraft Equipment Co., Ltd., Aviation Industry Corporation of China, Hefei 230051, China<sup>4</sup> School of Aeronautics, Nanjing University of Aeronautics and Astronautics, Nanjing 210007, China

\* Correspondence: shaolei@cqjtu.edu.cn

**Abstract:** Inert gas distribution has a great influence on the inerting effect, especially for the multiple-bay fuel tank. In order to find out the optimal scheme, an optimization method based on the entropy-weight improvement TOPSIS method is proposed, and an experimental system of inert gas distribution is established to measure the speed index and uniformity index. The results show that the position of the inlet and outlet has a significant effect on the overall inerting effect. The inerting scheme designed by the entropy-weight improvement TOPSIS method can not only reduce the flow demand of inert gas but also make the oxygen distribution more uniform. The optimization inerting scheme of the Boeing 747 aircraft has improved the average speed index by 3.01% and the average uniformity index by 26.18%. The smoke visualization experiment also showed that the scheme designed by the entropy-weight improvement TOPSIS method has the denser white smoke, which means that the scheme has better performance.

**Keywords:** inerting system; TOPSIS method; ventilation mode; optimization scheme



**Citation:** Shao, L.; He, J.; Lu, X.; Liu, W. Optimization Study of Inert Gas Distribution for Multiple-Bay Fuel Tank. *Processes* **2023**, *11*, 2441. <https://doi.org/10.3390/pr11082441>

Academic Editors: Iveta Marková and Ales Bernatik

Received: 5 July 2023

Revised: 31 July 2023

Accepted: 1 August 2023

Published: 14 August 2023



**Copyright:** © 2023 by the authors. Licensee MDPI, Basel, Switzerland. This article is an open access article distributed under the terms and conditions of the Creative Commons Attribution (CC BY) license (<https://creativecommons.org/licenses/by/4.0/>).

## 1. Introduction

Fire and explosion of aircraft fuel tanks is one of the major causes of catastrophic accidents [1]. Extensive development and analysis have shown that fuel tank inerting technology is an effective way to prevent fuel tank fires and explosions and enhances the survivability of an aircraft [2]. Fuel tank inerting technology refers to maintaining the ullage oxygen content below the limiting oxygen concentration (LOC), which does not support combustion; traditionally, the LOC is 9% or 12% for different aircraft [3]. Through development efforts, the onboard inert gas generation system (OBIGGS) has become the most effective way to reduce the oxygen concentration, by producing nitrogen enriched air (NEA) [4].

There are three key technologies in the design of OBIGGS: the air bleed and pretreatment system, air separation system, and inert gas distribution system. The main function of the air bleed and pretreatment system is to control the engine bleed at a suitable pressure and temperature range and remove harmful gases such as ozone [5]. The air separation system is mainly used for oxygen and nitrogen separation; the relatively mature technologies are the hollow fiber membrane technology and molecular sieve technology [6]. The inert gas distribution method refers to adjusting the schemes of vent ports and distributing NEA flow to achieve the purpose of vastly reducing the oxygen concentration in the fuel tank ullage [7].

The efficient distribution scheme of inert gas is critical for OBIGGS. It would be advantageous to inert the relatively irregular shape of the fuel tank with less venting systems and, as far as possible, to reduce cost and to simplify the system. In order to find out the best

scheme of the inert gas distribution of the Boeing 747SP, Cavage et al. established an engineering model for multiple-bay inerting, and full-scale fuel tank inert testing was adopted to verify the model. Feng et al. [8] established an ullage washing model of the B737 center wing tank and numerical analysis of two distribution schemes so that the non-uniform distribution could achieve the best inerting effect with the least amount of NEA. Burns et al. [9] conducted a flight test on the B747 central wing tank and measured the oxygen concentration of different bays; on this basis, the concept of “worst compartment” was defined to improve the inert gas distribution scheme. Wu et al. [10] established the inerting model of the multiple-bay fuel tank by using the computational fluid dynamics (CFD) method and compared different distribution schemes. In the research studies concerning distribution schemes, most are evaluated based on the average oxygen concentration.

However, due to space and function limitations, aircraft fuel tanks are usually designed in irregular shapes [11]. The existing evaluation system lacks the metric for assessing uniformity characteristics, so it cannot solve the problems of nonuniform distribution and insufficient inerting, especially on irregular multiple-bay fuel tanks [8]. Modern military inerting systems use a complex venting system to ensure a relatively uniform distribution of inert gas. Harris et al. [12] gave the definition of “hot spots” to describe the uniformity characteristics of fuel tank inerting, and a CFD model was established to identify “hot spots” oxygen distribution. The FAA conducted an inerting test on the A320 center wing tank, and eight gas sample ports were instrumented in the tank at different locations; the results showed that the maximum difference of oxygen concentration is more than 6%. In fact, the metric of average oxygen concentration can only represent the speed of inerting. For the purpose of scheme optimization, it is necessary to introduce the metric of uniformity into the evaluation system and establish a new optimization method.

The design of the inerting scheme is essentially an optimal solution process. The technique for order of preference by similarity to ideal solution (TOPSIS) is part of the analytical multi-criteria decision-making technique and has been widely used in the engineering field. Tavana et al. [13] adopted three different variations of TOPSIS including conventional, adjusted, and modified TOPSIS methods to determine the priority of manned space mission simulators, and all three TOPSIS methods arrived at the same solution. Chauhan et al. [14] evaluated the best performance of the impinging air jet released by the heat transfer surface in a rectangular channel with different indexes using an updated TOPSIS theory based on entropy weight. Kumar et al. [15] evaluated the optimal fuel combination in all internal combustion engine and pure diesel fuel mixtures using the enhanced TOPSIS theory based on entropy weight. Indeed, the modified TOPSIS approach is a multi-index comprehensive evaluation method based on entropy weight [16,17]. Because each assessment index has a different weight in the system, the weight of each index can be calculated scientifically and rationally and applied to the comprehensive evaluation of the best scheme.

In light of this, this work proposes an optimization method for irregular tank inerting systems based on the entropy-weight improvement TOPSIS method. The experimental platform for the fuel tank inerting system is established, and the smoke visualization experiment is utilized to validate the theoretical analysis. Finally, the various inerting schemes for the Boeing 747 CWT are compared by using the comprehensive evaluation method.

## 2. Optimization Method

The oxygen concentration in the fuel tank bay is in a gradient distribution, which means that the inerting scheme involving mixed nitrogen-rich gas should be evaluated according to the decrease rate of average oxygen concentration and the gradient of oxygen distribution. Therefore, it is necessary to define the velocity index and uniformity index. In this paper, the velocity index is defined as the time when the oxygen content in the fuel tank bay drops to 9%. Its evaluation process is consistent with the standard evaluation method [18,19]. The uniformity index can be calculated by the standard deviation of oxygen concentration in each compartment of the fuel tank. The standard deviation reflects the

dispersion of oxygen concentration. The more uniform the oxygen distribution is, the lower the standard deviation [20], which can be obtained by Equations (1) and (2):

$$\sigma = \sqrt{\frac{1}{N} \sum_{i=1}^N (h_i - \bar{h})^2} \quad (1)$$

$$\bar{h} = \frac{h_1v + h_2v + \dots + h_Nv}{V} \quad (2)$$

where  $N$  is the sample size;  $h_N$  is the sample value;  $\bar{h}$  is the mean value of samples;  $v$  is the volume of the discrete element;  $V$  is the space volume.

The final evaluation results of the inerting scheme are related to the size of the velocity index and the uniformity index. In order to calculate them, the entropy weight method is used to calculate the combined weight of the velocity index and uniformity index. The evaluation index matrix  $X$  can be generated by integrating several methods of the speed and uniformity index:

$$X = (x_{ij})_{m \times n} = \begin{pmatrix} x_{11} & x_{12} & \dots & x_{1n} \\ x_{21} & x_{22} & \dots & x_{2n} \\ \vdots & \vdots & \dots & \vdots \\ x_{m1} & x_{m2} & \dots & x_{mn} \end{pmatrix} \quad (3)$$

where  $x_{ij}$  is the evaluation indicator  $j$  for the  $i$  evaluation object;  $m$  is the evaluation object;  $n$  is the evaluating index.

Because the two types of indicators involve different contents, it is necessary to homogenize the original data. The results are obtained by Equations (4)–(7):

$$A = \max(x_{1j}, x_{2j}, \dots, x_{mj}) \quad (4)$$

$$B = \min(x_{1j}, x_{2j}, \dots, x_{mj}) \quad (5)$$

$$y_{ij}^+ = \frac{x_{ij} - B}{A - B} \quad (6)$$

$$y_{ij}^- = \frac{A - x_{ij}}{A - B} \quad (7)$$

The larger value of the positive index  $y_{ij}^+$ , the better the normalization effect is. The smaller value of the inverse index  $y_{ij}^-$ , the better the normalization effect is. Due to the different dimensions between the indicators, the data after assimilation need to be normalized as follows [21]:

$$P_{ij} = \frac{y_{ij}}{\sum_{i=1}^m y_{ij}^{\pm}} = \begin{pmatrix} P_{11} & P_{12} & \dots & P_{1n} \\ P_{21} & P_{22} & \dots & P_{2n} \\ \vdots & \vdots & \dots & \vdots \\ P_{m1} & P_{m2} & \dots & P_{mn} \end{pmatrix} \quad (8)$$

where  $P_{ij}$  is the proportion of the  $i$  evaluation object in the  $j$  index;  $m$  is the evaluation object;  $n$  is the evaluation index.

The entropy value  $E_j$  of each index can be obtained via Equation (9):

$$E_j = -\frac{\sum_{i=1}^m P_{ij} \ln P_{ij}}{\ln m} \quad (9)$$

Therefore, entropy weight  $W_j$  is:

$$W_j = \frac{1 - E_j}{\sum_{j=1}^n 1 - E_j} \quad (10)$$

After the entropy weights of the speed index and the uniformity index are obtained by Equations (8)–(10), they are substituted into the TOPSIS method for multi-index comprehensive evaluation. First, the original data is normalized to obtain the matrix  $C_{ij}$ , and then the weighted matrix  $Z_{ij}$  is constructed:

$$C_{ij} = \frac{x_{ij}}{\sqrt{\sum_{i=1}^m (x_{ij})^2}} \quad (11)$$

$$Z_{ij} = C_{ij}W_j \quad (12)$$

where  $Z_{ij}$  is the multiplication of  $C_{ij}$  and weight  $W_j$ ; positive ideal value  $D^+$  and negative ideal value  $D^-$  based on weighted matrix  $Z_{ij}$  are as follows:

$$D^+ = \{\max |Z_{i1}, Z_{i2}, \dots, Z_{in}\}, i = 1, 2 \dots m \quad (13)$$

$$D^- = \{\min |Z_{i1}, Z_{i2}, \dots, Z_{in}\}, i = 1, 2 \dots m \quad (14)$$

Then, the positive Euclidean distance and negative Euclidean distance of each index are calculated. The formula is as follows:

$$D_i^+ = \sqrt{\sum_{j=1}^n (Z_{ij} - D^+)^2} \quad (15)$$

$$D_i^- = \sqrt{\sum_{j=1}^n (Z_{ij} - D^-)^2} \quad (16)$$

Finally, the ideal point distance  $C_i$  is calculated by Equation (17). Then, the tank circulation mode is evaluated and classified according to  $C_i$ . Because the velocity index and uniformity index are positive, the smaller the ideal point distance  $C_i$ , the better the inert gas flow in the tank is:

$$C_i = \frac{D_i^-}{D_i^- + D_i^+} \quad (17)$$

### 3. Experimentation and Methodology

In order to provide the original calculation data for the evaluation method, the nitrogen-rich gas inerting experiment was designed. The detailed dimensions of the Boeing 747 CWT are obtained by referring to Cavage [22]. The CWT is an asymmetric fuel tank with a length of 6.15 m, a width of 6.48 m, and a height of 1.98 m to 1.22 m. It has a nitrogen-rich inlet and two nitrogen-rich outlets. The interior is composed of six bays, and the connection and size between each bay are different. The details are shown in Figure 1a. In order to simulate the distribution of inert gases in the Boeing 747 CWT, a scale CWT model was constructed using plywood according to the drawings in the National Transportation Safety Board (NTSB). In the report, the scale modeling of the 747-100 CWT is described in detail [23]. The tank length ratio is 10%. There are holes between the partitions of the tank model to allow the free flow of nitrogen-rich gas. Each spanwise beam and some ribs are also scaled in the same proportion, and all penetration holes are merged into the geometric center of the plane and scaled according to the relative area. Each bay of the tank has a gas sampling port at the top of the geometric center. In order to prevent leakage of the petrol tank model and ensure its air tightness, glue and tape are used to seal the model. The battery oxygen sensor is used to measure the change in oxygen concentration and transmit data to the data recorder.

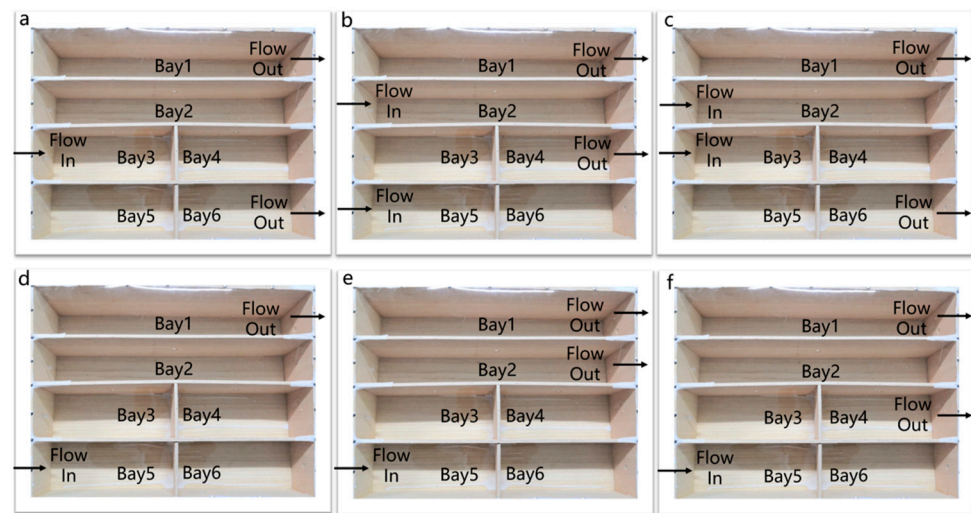


**Figure 1.** Optimization scheme of inlet and outlet positions for inerting system. (a) Original scheme; (b) Scheme 1; (c) Scheme 2; (d) Scheme 3; (e) Scheme 4; (f) Scheme 5.

Therefore, when designing the inerting system, the length of the flow channel should be increased as much as possible to prolong the residence time of the nitrogen-rich gas in the fuel tank and enhance the inerting effect. According to the above principle, five new inerting schemes are designed by changing the gas inlet and outlet positions of the fuel tank, as show in Figure 1.

Six experiments were carried out according to the six designed inerting schemes. The installation of the experimental equipment is shown in Figure 2. Before the experiment, the tank was made according to the inerting scheme, then all the equipment was connected, and finally the air tightness of the pipeline interface and the tank model was checked.

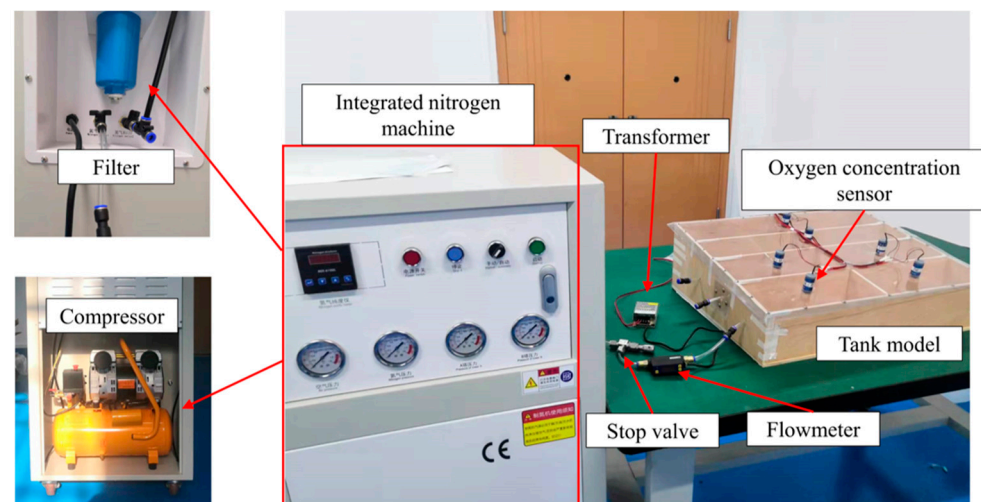


**Figure 2.** Experimental system.

After all devices are connected, the power supply is first connected to turn on the compressor and the nitrogen generator. Then, the stop valve between the nitrogen generator and the external environment is opened to pre-inert the nitrogen generator. When the oxygen concentration sensor connected to the exhaust pipe of the nitrogen generator detects that the oxygen concentration drops to 5%, the pre-inerting process is completed. Next, the stop valve connected to the external environment is closed, the stop valve connected to the tank model is opened, and the flow valve to control the nitrogen-rich gas flow into the tank model is adjusted. At this time, the data recorder begins to record the output data

and inerting time of the oxygen concentration sensors in the six bays. Finally, when the oxygen concentration in all bays is lower than 9%, the inerting is stopped, the compressor, the nitrogen generator and the stop valve connected to the tank model are closed, the stop valve connected to the external environment is opened, and the experimental process of the scheme is completed. The fuel tank inerting experiment diagram is shown in Figure 3.

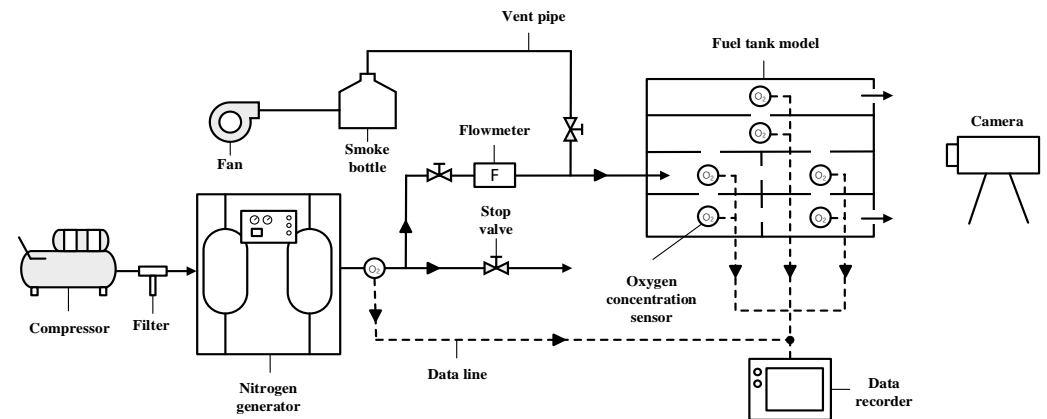


**Figure 3.** Schematic of the experimental equipment.

Only one inerting scheme will be implemented in each experimental operation. Therefore, in order to eliminate the effects of the previous experiment, it is necessary to ventilate the tank model before implementing another scheme. After all the inerting schemes are tested, the device power supply is turned off, and the data collected by the data recorder instrument is sorted. During the experiments, the monitoring data using the oxygen concentration sensor will be captured and stored in the computer using a data logger and software.

In order to facilitate the verification of the variation of oxygen concentration in the inerting flow field of multi-bay fuel tanks, this paper adds equipment such as fans, smoke boxes, and cameras to conduct smoke visualization experiments on the optimization scheme and the original scheme. Figure 3 shows the attachment of the experimental equipment. In the experiment, the smoke cake with moderate smoke volume and obvious display was placed in the smoke box as the smoke generation material, and then the inlet of the fan, smoke box, and fuel tank model was connected through the vent pipe, where the vent pipe was equipped with a stop valve. The fuel tank model outlet is connected to the outdoor environment through a vent duct. Since the smoke is white, black paper is glued to the bottom of the petrol tank model to make the image more easily collected by the camera. Finally, the camera is used to capture the smoke flow process in two different fuel tank models.

After the device is connected, the smoke cake is ignited. The fan is opened when the smoke flow is stable, and the speed control knob of the fan is adjusted to achieve various wind speeds. Then, the stop valve connecting the fuel tank model is opened, and the smoke enters the fuel tank model with the air flow. At this time, the smoke flow trajectory is captured by the camera. The experiment starts from the fan work, and the continuous shooting interval of the camera is 15 s. The total shooting time of the camera is consistent with the burning time of the smoke cake, which is about 2 min. After completing an experiment, the smoke cake in the smoke box needs to be cleaned, and the remaining smoke in the pipe and tank model needs to be blown away by the fan. Next, the experiment of the next scheme is carried out according to the above steps. After the test of all schemes is completed, the fan and the stop valve connecting the fuel tank model are closed, the smoke cake in the smoke box is removed, and the image recorded by the camera is obtained.

During the experiment, due to the accuracy of the measuring equipment, human error, test time, and other factors, the experimental data collection may be inaccurate. By referring to the equipment uncertainty analysis in the relevant literature, all the measuring devices

used in the experiment were calibrated [24]. Table 1 shows the uncertainty analysis results of various parameters considered in this study.

**Table 1.** Uncertainty value of various parameters.

Measured Quantity	Uncertainty/%
Nitrogen purity	±1
Oxygen concentration	±1
Flowmeter	±1.5
Data recorder readings	±2
Fan speed	±5

#### 4. Results and Discussions

The initial oxygen concentration of the above schemes is set to 21%, and the real-time oxygen concentration change data of the six schemes are obtained through experiments, as shown in Figure 4.

In order to summarize the change in oxygen concentration in the figure, the original data are normalized, and the velocity index and uniformity index of the six schemes are obtained. The results are shown in Tables 2 and 3.

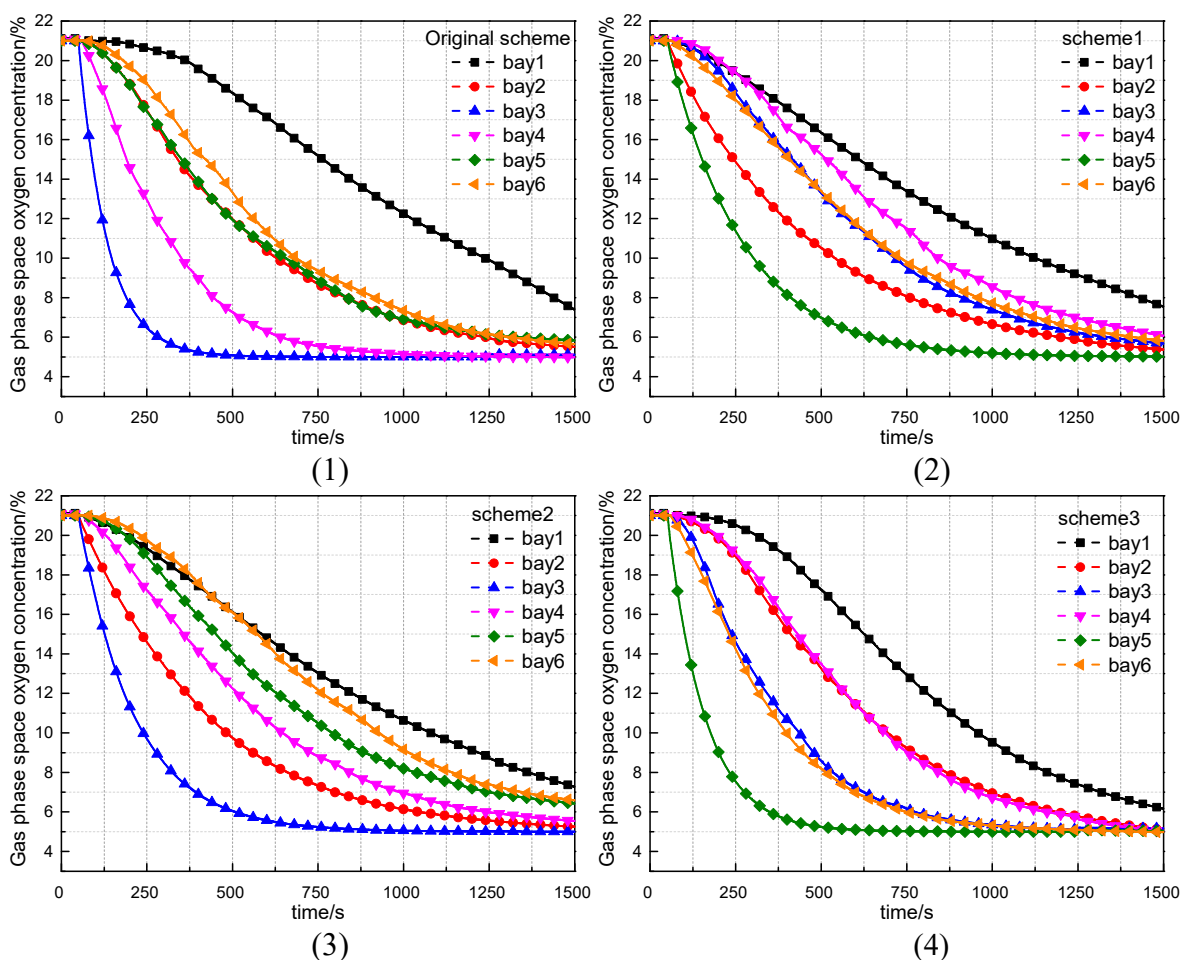


**Figure 4.** Cont.

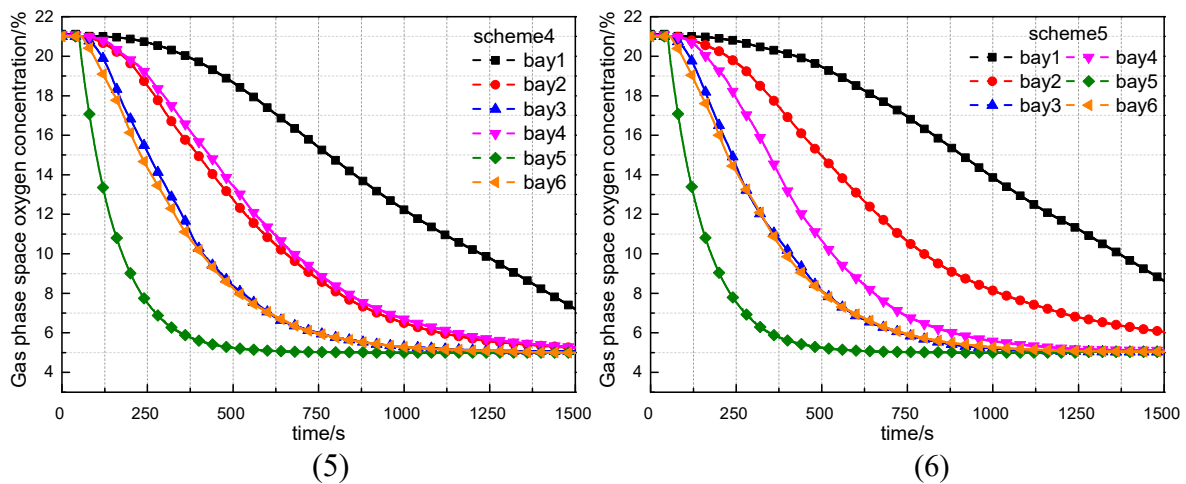


Figure 4. Experimental results notes: (1) Original scheme; (2) Scheme 1; (3) Scheme 2; (4) Scheme 3; (5) Scheme 4; (6) Scheme 5.

Table 2. Speed index of each scheme.

Scheme	Bay1/s	Bay2/s	Bay3/s	Bay4/s	Bay5/s	Bay6/s
original scheme	1340	727	173	408	747	790
1	1277	631	795	956	349	849
2	1224	567	280	731	886	1014
3	1056	771	481	751	210	452
4	1331	732	464	754	204	462
5	1470	890	461	590	203	445

Table 3. Uniformity index of each scheme.

Scheme	Bay1 /10 <sup>-3</sup>	Bay2 /10 <sup>-3</sup>	Bay3 /10 <sup>-3</sup>	Bay4 /10 <sup>-3</sup>	Bay5 /10 <sup>-3</sup>	Bay6 /10 <sup>-3</sup>
original scheme	4.683	5.432	0.004	0.597	3.191	3.134
1	4.267	4.049	3.983	3.961	0.795	7.025
2	6.589	3.303	0.251	5.717	4.007	5.221
3	2.458	6.121	0.775	4.475	0.015	1.24
4	5.182	4.245	0.856	4.561	0.018	1.264
5	4.847	4.784	0.666	1.287	0.018	0.978

As shown in Tables 3 and 4, we can find the following phenomena by comparing different experimental schemes. In scheme 1, compared with the original scheme, the gas inlet is farther away from bay 3, which reduces the decline rate of oxygen concentration, and the velocity index decreased by 398 s. In addition, bay 5 is the gas outlet, which makes the concentration decrease faster, and the velocity index increases by 622 s. In scheme 2, the uniformity index of the compartment is larger than that of other schemes, and the average value is  $4.181 \times 10^{-3}$ . The far distribution between the gas outlets may be the cause of this phenomenon. In scheme 3, there is only one air inlet, which makes the oxygen concentration of bay 5 decrease the fastest among all bays, and the velocity index is 210 s. Its uniformity index reaches the minimum value of  $0.015 \times 10^{-3}$  in all schemes. In scheme 4, compared with scheme 3, an air inlet is added at bay 2. This led to a decrease in its velocity index by 39 s and a decrease in the uniformity index by  $1.876 \times 10^{-3}$ . Increasing the gas inlet will accelerate the rate of change in oxygen concentration, and it will also reduce the oxygen concentration of the bay. In scheme 5 and scheme 4, the oxygen concentration velocity index and uniformity index of bay 3, bay 5, and bay 6 are close. This may mean that when the position of the gas outlet does not change much, the bay near the gas inlet can remain stable.



**Table 4.** Entropy value and entropy weight of each index.

Index	Entropy Value $e_j$	Entropy Weight $w_j$	Index	Entropy Value $e_j$	Entropy Weight $w_j$
Bay 1 velocity	0.997	0.002	Bay 1 uniformity	0.979	0.016
Bay 2 velocity	0.994	0.005	Bay 2 uniformity	0.989	0.009
Bay 3 velocity	0.944	0.043	Bay 3 uniformity	0.660	0.263
Bay 4 velocity	0.982	0.014	Bay 4 uniformity	0.901	0.077
Bay 5 velocity	0.889	0.086	Bay 5 uniformity	0.548	0.350
Bay 6 velocity	0.968	0.025	Bay 6 uniformity	0.857	0.111

The evaluation index matrix  $X$  of the six schemes is generated by combining the data in Tables 2 and 3, and then the entropy value and entropy weight of each index can be calculated by Equations (4)–(10). The results are shown in Table 4. Finally, based on the data in Table 4, the comprehensive evaluation results can be obtained by Equations (11)–(17), as shown in Table 5.

**Table 5.** Comprehensive evaluation results.

Scheme	$D_i^+$	$D_i^-$	$C_i$	Ranking
original scheme	0.263	0.219	0.454	4
1	0.220	0.267	0.547	6
2	0.235	0.282	0.545	5
3	0.346	0.059	0.145	2
4	0.343	0.063	0.156	3
5	0.352	0.043	0.109	1

In Table 4, the entropy weight of the velocity index and the entropy weight of the uniformity index of the compartment are given. After observing the data in the table, it can be found that there is a huge gap in the entropy weight of the speed index between bay 1 and bay 5. The reason for this phenomenon may be due to the large volume of bay 1, which is more than twice that of bay 5. In addition, in most schemes, the direct connection of the air inlet to bay 5 is also an important reason. According to the evaluation results in Table 5, the order of inerting performance is as follows: scheme 5 > scheme 3 > scheme 4 > original scheme > scheme 2 > scheme 1. The relative proximity of the original scheme is 0.454, ranking fourth. The relative closeness of the optimal solution scheme 5 is 0.109, ranking first. The reason for this is that the longer flow channel of scheme 5 allows the nitrogen-rich gas to stay in the fuel tank for a longer time and provides more air replacement. In addition, it can be seen from Table 6 that, compared with the original scheme, the average speed index has increased by 3.01%, and the average uniformity index has increased by 26.18%; the average speed and uniformity indexes are calculated by comparing the averages of Tables 2 and 3, indicating that scheme 5 not only reduces the demand for inerting gas flow, but also makes the oxygen concentration distribution more uniform.

**Table 6.** Performance increase.

Scheme	Average Speed Index Increasing Rate/%	Average Uniformity Index Increasing Rate/%
1	−16.06	−41.31
2	−12.35	−47.22
3	11.09	11.48
4	5.69	5.37
5	3.01	26.18

In order to verify the inerting effect of the optimized scheme 5, the smoke visualization experiment was carried out by simulating the real external environment, and then the air flow changes in each bay during the experiment were observed. In the experiment, after

shooting with the camera for 2 min, the airflow photos of scheme 5 are compared with the original scheme, as shown in Figure 5. By comparing the flue gas distribution in the two schemes, it can be seen that the flue gas in the bay of scheme 5 is denser and richer, which indicates that the inerting speed of scheme 5 is faster and more uniform. By comparing the flue gas distribution of the two methods at the same time, it is clear that the smoke in the bay of scheme 5 is denser and richer, indicating that scheme 5's inerting speed is both faster and more uniform. By comparing the flue gas distribution in the two schemes, it can be seen that the flue gas in the bay of scheme 5 is denser and richer, which indicates that the inerting speed of scheme 5 is faster and more uniform. The flue gas concentration of the original scheme is not high, which is more obvious in bay 1, which is difficult to inert. As shown in Figure 5c, the flue gas distribution in the upper left corner is sparse. However, compared with the original scheme, the smoke distribution concentration in bay 1 in scheme 5 is higher and more uniform, as shown in Figure 5f.

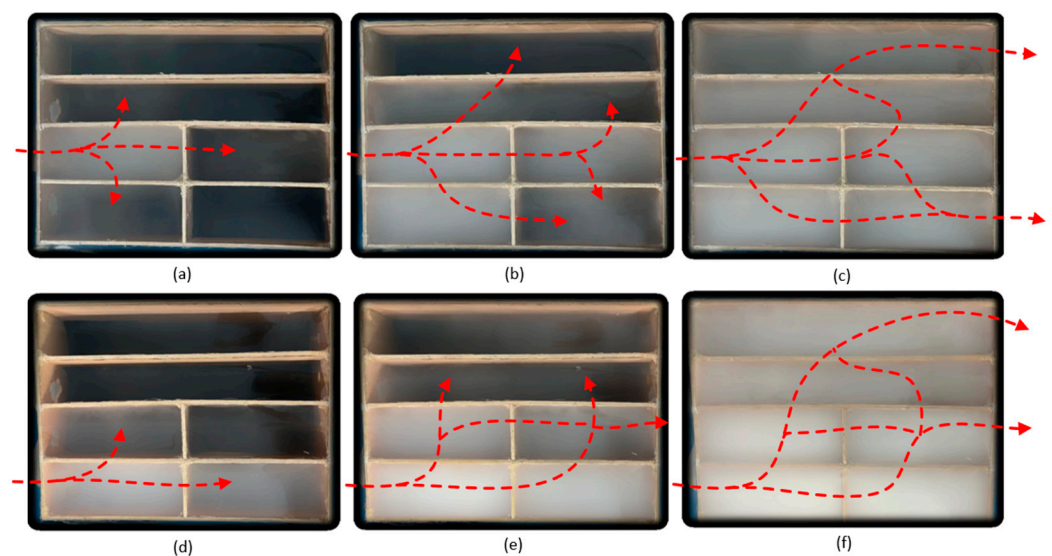


**Figure 5.** Comparison of airflow between the original and scheme 5; (a) Original scheme 30 s; (b) Original scheme 90 s; (c) Original scheme 120 s; (d) Scheme 5 30 s; (e) Scheme 5 90 s; (f) Scheme 5 120 s.

The flow process of smoke indicates that the smoke mainly diffuses along the connection path between the gas inlet and the gas outlet. On the other hand, by observing Figure 5b,e, it can be found that the smoke of scheme 5 is denser and more average when it is finally stable, but the original scheme seems to diffuse faster in different bays during the diffusion process. This may be due to the shorter distance between the gas inlet and the gas outlet in the original scheme. In summary, in the process of fuel tank design, the gas inlet and the gas outlet of the fuel tank should be diagonally designed to improve the inerting speed, and the distance between the two should also be considered to improve the inerting effect.

In the field of fuel tank inerting, many people have conducted a lot of work, such as Cavage [24], who designed a multi-compartment inert gas distribution model; Feng [8] constructed the empty cabin flushing model of the central wing tank; Burns established the 'worst cabin' inert gas distribution scheme; Wu [10] designed a multi-compartment fuel tank inerting model. However, most of these studies are evaluated based on a single average oxygen concentration, which means that the evaluation results can only be applied to the overall assessment, and the changes in details (such as uniformity of oxygen concentration) cannot be reflected. In view of these limitations, we use the speed index and the uniformity index to evaluate the effect of the scheme. By summarizing the experimental results, scheme 5 can be determined as a better inerting scheme. Compared with the original scheme, the smoke distribution effect of scheme 5 is improved, and the inerting effect is optimized.

In fact, there may be more schemes for the inlet and outlet, so scheme 5 may be not the best, but it may be relatively better. The impact of samples on entropy weight is actually a universal problem [25,26]; Bao et al. [27] found that under different sample conditions, the entropy weight method cannot accurately reflect the information content and discriminability of indexes. Sahoo et al. [28] and Yang et al. [29] assigned weights according to the discriminating degree of indicators: the results showed that a higher discrete degree corresponds to a larger weight requirement. The impact of samples on entropy weight really requires further research.

## 5. Conclusions

In this paper, a TOPSIS method suitable for the inerting system of irregular fuel tanks is established. The inerting scheme of the Boeing 747 center wing fuel tank is designed and comprehensively evaluated with the TOPSIS method, and the optimal design of the inerting scheme is realized.

The position of the inlet and outlet has a significant effect on the overall inerting effect of the fuel tank under the same working conditions. The optimized inerting scheme is superior to the original design in terms of inerting speed and uniformity of oxygen concentration distribution in the gas phase space.

The optimization inerting scheme of the Boeing 747 aircraft has improved the speed index by 3.01% and the uniformity index by 26.18%.

The optimization of inert gas distribution in multi-compartment fuel tanks provides a new inerting optimization method for the B747 CWT. Compared with the traditional fuel tank inerting scheme, inert gas distribution is more uniform, and the inerting effect is better. The conclusions can provide theoretical support for the optimal design of the fuel tank inerting schemes. In future work, we will further study the influence of the distribution of compartments in the fuel tank on the inerting effect.

**Author Contributions:** Article writing, experimental design, and image acquisition, L.S.; writing—original draft preparation, J.H.; formal analysis, X.L.; project administration, W.L. All authors have read and agreed to the published version of the manuscript.

**Funding:** This work was supported by the National Natural Science Foundation of China—Civil Aviation Research Fund (No.U1933121), the Research Fund of Key Laboratory of Aircraft Environment Control and Life Support, MIIT, Nanjing University of Aeronautics and Astronautics (No.KLAECLS-E-202002), the Science and Technology Research Program of Chongqing Municipal Education Commission (No.KJQN201900738), Natural Science Foundation of Chongqing, China (CSTB2022NSCQ-MSX1301).

**Data Availability Statement:** All data and materials generated or analyzed during this study are included in this published article.

**Conflicts of Interest:** The authors declare no conflict of interest.

## References

1. Reynolds, T.L.; Eklund, T.I.; Haack, G.A. *Onboard Inert Gas Generation System/Onboard Oxygen Gas Generation System (Obiggs/Obogs) Study, Part 2: Gas Separation Technology-State of the Art*; NASA Center for Aerospace Information: Hanover, MD, USA, 2001.
2. Aryal, U.R.; Chouhan, A.; Darling, R.; Yang, Z.; Perry, M.L.; Prasad, A.K. Electrochemical gas separation and inerting system. *J. Power Sources* **2021**, *501*, 229959. [[CrossRef](#)]
3. Boeing Phantom Works. *Report No.: NASA/CR 2001-210950*; Boeing Phantom Works: Seattle, WA, USA, 2001.
4. Summer, S.M. *Mass Loading Effects on Fuel Vapor Concentration in an Aircraft Fuel Tank Ullage*; US Department of Transportation, Federal Aviation Administration: Cambridge, MA, USA, 1999.
5. Federal Aviation Administration. *Report No.: DOT/FAA/AR-TN99/65*; Federal Aviation Administration: Atlantic, NJ, USA, 1999.
6. Li, G.; Kujawski, W.; Válek, R.; Koter, S. A review—The development of hollow fibre membranes for gas separation processes. *Int. J. Greenh. Gas Control*. **2021**, *104*, 103195.
7. Keim, M.; Kalló, J.; Friedrich, K.A.; Werner, C.; Saballus, M.; Gores, F. Multifunctional fuel cell system in an aircraft environment: An investigation focusing on fuel tank inerting and water generation. *Aerosp. Sci. Technol.* **2013**, *29*, 330–338. [[CrossRef](#)]
8. Feng, S.; Li, C.; Peng, X.; Wen, T.; Yan, Y.; Jiang, R.; Liu, W. Oxygen concentration variation in ullage influenced by dissolved oxygen evolution. *Chin. J. Aeronaut.* **2020**, *33*, 1919–1928. [[CrossRef](#)]

9. Burns, M.; Cavage, W.M.; Hill, R.; Morrison, R. *Flight-Testing of the FAA Onboard Inert Gas Generation System on an Airbus A320*; Report No.: DOT/FAA/AR-03/58; Federal Aviation Administration: Atlantic, NJ, USA, 2004.
10. Wu, F.; Lin, G.; Zeng, Y.; Pan, R.; Sun, H. Experimental Study of an On-board Fuel Tank Inerting System. *IOP Conf. Ser. Mater. Sci. Eng.* **2017**, *187*, 012010. [[CrossRef](#)]
11. Lind, I.; Oprea, A. Detailed geometrical information of aircraft fuel tanks incorporated into fuel system simulation models. In Proceedings of the 9th International MODELICA Conference, Munich, Germany, 3–5 September 2012; pp. 333–338.
12. Harris, A.P.; Ratcliffe, N.M. Dimensional modelling of the fuel outgassing phenomenon: Improving flammability assessment of aircraft fuel tanks. *Aeronaut. J.* **2011**, *115*, 605–614. [[CrossRef](#)]
13. Tavana, M.; Hatami-Marbini, A. A group AHP-TOPSIS framework for human spaceflight mission planning at NASA. *Expert Syst. Appl.* **2011**, *38*, 13588–13603. [[CrossRef](#)]
14. Chauhan, R.; Singh, T.; Tiwari, A.; Patnaik, A.; Thakur, N.S. Hybrid entropy—TOPSIS approach for energy performance prioritization in a rectangular channel employing impinging air jets. *Energy* **2017**, *134*, 360–368. [[CrossRef](#)]
15. Kumar, C.; Rana, K.B.; Tripathi, B. Performance evaluation of diesel-additives ternary fuel blends: An experimental investigation, numerical simulation using hybrid Entropy–TOPSIS method and economic analysis. *Therm. Sci. Eng. Prog.* **2020**, *20*, 100675. [[CrossRef](#)]
16. Chodha, V.; Dubey, R.; Kumar, R.; Singh, S.; Kaur, S. Selection of industrial arc welding robot with TOPSIS and Entropy MCDM techniques. *Mater. Today Proc.* **2022**, *50*, 709–715. [[CrossRef](#)]
17. Huang, W.; Wu, M.; Chen, L.; Chen, X.; Cao, W. Multi-objective drilling trajectory optimization using decomposition method with minimum fuzzy entropy-based comprehensive evaluation. *Appl. Soft Comput.* **2021**, *107*, 107392. [[CrossRef](#)]
18. Cai, Y.; Bu, X.; Lin, G.; Sun, B.; Zeng, Y.; Li, Z. Experimental study of an aircraft fuel tank inerting system. *Chin. J. Aeronaut.* **2015**, *28*, 394–402. [[CrossRef](#)]
19. Renouard-Vallet, G.; Saballus, M.; Schumann, P.; Kallo, J.; Friedrich, K.A.; Müller-Steinhagen, H. Fuel cells for civil aircraft application: On-board production of power, water and inert gas. *Chem. Eng. Res. Des.* **2012**, *90*, 3–10. [[CrossRef](#)]
20. Sindhu, A.; Radha, V. A Method for Removing PET/CT Imaging Artifact Using Combination of Standard Deviation and Computational Geometry Technique. *Procedia Comput. Sci.* **2020**, *167*, 969–978. [[CrossRef](#)]
21. Peters, R.; Samsun, R.C. Evaluation of multifunctional fuel cell systems in aviation using a multistep process analysis methodology. *Appl. Energy* **2013**, *111*, 46–63. [[CrossRef](#)]
22. Cavage, W. Modeling Inert Gas Distribution in Commercial Transport Aircraft Fuel Tanks. In Proceedings of the 22nd AIAA Aerodynamic Measurement Technology and Ground Testing Conference, St. Louis, MO, USA, 24–26 June 2002; American Institute of Aeronautics and Astronautics: St. Louis, MO, USA, 2002. [[CrossRef](#)]
23. Shepherd, J.E.; Krok, J.C.; Lee, J.J.; Birky, M.M.; Plaza, L. *Jet A Explosions—Field Test Plan; 1/4 Scale Experiments*; California Institute of Technology: Pasadena, CA, USA, 1997; Volume 66.
24. Cavage, W.M.; Kils, O. *Inerting a Boeing 747SP Center Wing Tank Scale Model with Nitrogen-Enriched Air*; Report No.: DOT/FAA/AR-02/51; Federal Aviation Administration: Atlantic, NJ, USA, 2002.
25. Kacprzak, D. A doubly extended TOPSIS method for group decision making based on ordered fuzzy numbers. *Expert Syst. Appl.* **2019**, *116*, 243–254. [[CrossRef](#)]
26. Dutta, B.; Dao, S.D.; Martínez, L.; Goh, M. An evolutionary strategic weight manipulation approach for multi-attribute decision making: TOPSIS method. *Int. J. Approx. Reason.* **2021**, *129*, 64–83. [[CrossRef](#)]
27. Bao, Q.; Yuxin, Z.; Yuxiao, W.; Feng, Y. Can Entropy Weight Method Correctly Reflect the Distinction of Water Quality Indices? *Water Resour. Manag.* **2020**, *34*, 3667–3674. [[CrossRef](#)]
28. Sahoo, M.M.; Patra, K.C.; Swain, J.B.; Khatua, K.K. Evaluation of water quality with application of Bayes' rule and entropy weight method. *Eur. J. Environ. Civ. Eng.* **2017**, *21*, 730–752. [[CrossRef](#)]
29. Yang, J.; Chang, J.; Wang, Y.; Li, Y.; Hu, H.; Chen, Y. Comprehensive drought characteristics analysis based on a nonlinear multivariate drought index. *J. Hydrol.* **2017**, *557*, 651–667. [[CrossRef](#)]

**Disclaimer/Publisher's Note:** The statements, opinions and data contained in all publications are solely those of the individual author(s) and contributor(s) and not of MDPI and/or the editor(s). MDPI and/or the editor(s) disclaim responsibility for any injury to people or property resulting from any ideas, methods, instructions or products referred to in the content.